



et al., 2011). Distributed numerical simulations are an effective, process-based method for predicting groundwater resources and quality (Rehrl and Birk, 2010). Teutsch and Sauter (1991) give an overview of the basic modelling concepts applicable for simulating karst aquifers. The geometry of the karst conduit system can be approximated with hybrid models, which simulate the fast flow component in the highly conductive karst conduit system in discrete one-dimensional elements and couple it to a two- or three-dimensional continuum representing the fissured matrix of the aquifer (Oehlmann et al., 2013). Hybrid models are rarely applied to real karst systems because they have a high demand of input data (Reimann et al., 2011). They are however regularly applied in long-term karst genetic simulation scenarios (e.g. Clemens et al., 1996; Bauer et al., 2003; Hubinger and Birk, 2011). In these models not only groundwater flow but also solute transport is coupled in the fissured matrix and in the karst conduits. Aside from karst evolution such coupling enables models to simulate tracer or contaminant transport in the karst conduit system (e.g. Birk et al., 2005). In addition to serving for predictive purposes, such models can be used for providing information about the groundwater catchment itself (Rehrl and Birk, 2010).

A major problem for characterizing the groundwater system with numerical models is generally the model ambiguity. A large number of calibration parameters is usually opposed by a relatively low number of field observations leading to several parameter combinations, which give the same fit to the observed data but sometimes very different results for prognostic simulations (Li et al., 2009). It is well known that the use of several objective functions, i.e. several independent field observations, can significantly reduce the amount of plausible parameter combinations (Ophori, 1999). Especially in hydrology (e.g. Khu et al., 2008; Hunter et al., 2005) but also for groundwater systems (e.g. Ophori, 1999; Hu, 2011) this approach has been successfully applied with a wide range of observation types, e.g. groundwater recharge, hydraulic heads, remote sensing, solute transport, etc. (Ophori, 1999; Li et al., 2009; Hu, 2011). Usually, automatic calibration schemes performing a multi-objective calibration for several parameters are used for this purpose (Khu et al., 2008). However, calculation times are

9283

large due to the high amount of model runs needed (Khu et al., 2008) and a precise and well-understood conceptual model is essential as basis for the automatic calibration (Madsen, 2003). Numerical models of karst aquifers are difficult to build because of their highly developed heterogeneity (Rehrl and Birk, 2010). Especially the geometric and hydraulic properties of the karst conduit system are usually unknown and difficult to characterize with field experiments (Worthington, 2009). With artificial tracer test data the maximum conduit volume can be estimated but an unknown contribution of fissured matrix water prevents further conclusion on conduit geometry (Birk et al., 2005).

For a distributed simulation of the total aquifer system including the fissured matrix and the karst conduit system rather advanced numerical models are necessary, which are not suited for multi-objective calibration due to long simulation times and complex parameter interdependence. Therefore, numerical models of karst areas usually cannot simulate the hydraulic head distribution in the area, spring discharge and tracer breakthrough curves simultaneously on catchment scale. Some studies combine groundwater flow with particle-tracking for tracer directions (e.g. Worthington, 2009) without simulating tracer transport. On the other hand there are studies simulating breakthrough curves without calibrating for measured hydraulic heads (e.g. Birk et al., 2005). For developing process-based models which can be used as prognostic tools e.g. for delineation of protection zones, the simulation should be able to reproduce groundwater flow and transport within a groundwater catchment. Especially in complex hydrogeological systems, this approach would reduce model ambiguity, which is a prerequisite in predicting groundwater resources and pollution risks (Birk et al., 2005).

This study shows how the combination of groundwater flow and transport simulation can be used not only to develop a basis for further prognostic simulations in a heterogeneous karst aquifer on catchment scale but also to reduce model ambiguity and draw conclusions on karst network geometries and the actual karst conduit volume. The approach shows the kind and minimum amount of field observations needed for this aim. Furthermore, a systematic calibration strategy is presented to reduce the amount of necessary model runs and the simulation time compared to standard multi-objective

9284

calibrations. For this purpose a hybrid model was built and a pattern matching procedure was applied for a well-studied karst aquifer system in south western Germany. The model was calibrated for three major observed parameters: the hydraulic head distribution derived from measurements in 20 boreholes, the spring discharge of six springs and the tracer breakthrough curves of two tracer tests.

## 2 Modelling approach

The simulation is based on the mathematical flow model discussed in detail by Oehlmann et al. (2013). The authors set up a three-dimensional hybrid model for groundwater flow with the software Comsol Multiphysics<sup>®</sup>. As described by Oehlmann et al. (2013) the simulation was conducted simultaneously in the three-dimensional fissured matrix, in an individual two-dimensional fault zone and in one-dimensional karst conduit elements to account for the heterogeneity of the system. Results showed that the karst conduits widen towards the springs and therefore a linear relationship between the conduit radius and the conduit length  $s$  [L] was established. Values for  $s$  start with zero at the point farthest away from the spring and increase towards the respective karst spring. In agreement with these results and karst genesis simulations by Liedl et al. (2003), the conduit radius is calculated as:

$$r_c = ms + b \quad (1)$$

$r_c$  [L] is the radius of a conduit branch and  $m$  and  $b$  are the two parameters defining the conduit size.  $b$  [L] is the initial radius of the conduit at the point farthest away from the spring and  $m$  [-] is the slope with which the conduit radius increases along the length of the conduit  $s$ .

In the following the equations used for groundwater flow and transport are described. The subscript  $m$  denotes the fissured matrix,  $f$  the fault zone and  $c$  the conduits hereby allowing a clear distinction between the respective parameters. Parameters without a subscript are the same for all karst features in the model.

9285

### 2.1 Groundwater flow

Groundwater flow was simulated for steady-state conditions. This approach seems appropriate since this work focuses on the simulation of tracer transport in the conduit system during tracer tests, which are ideally conducted under quasi-steady state flow conditions. The groundwater flow in the three-dimensional fissured matrix was simulated with the continuity equation and the Darcy equation (Eq. 2a und b).

$$Q_m = \nabla(\rho \mathbf{u}_m) \quad (2a)$$

$$\mathbf{u}_m = -K_m H_m \quad (2b)$$

with  $Q_m$  being the mass source term [ML<sup>-3</sup>T<sup>-1</sup>],  $\rho$  the density of water [ML<sup>-3</sup>] and  $\mathbf{u}_m$  the Darcy velocity [LT<sup>-1</sup>]. In Eq. (2b)  $K_m$  is the hydraulic conductivity of the fissured matrix [LT<sup>-1</sup>] and  $H_m$  the hydraulic head [L].

Two-dimensional fracture flow in the fault zone was simulated with Comsol's<sup>®</sup> Fracture Flow Interface. The interface only allows for the application of the Darcy equation inside of fractures, so laminar flow in the fault zone was assumed. In order to obtain a better process-based conceptualization of flow, the hydraulic fault conductivity  $K_f$  was calculated by the cubic law (Eq. 3):

$$K_f = \frac{d_f^2 \rho g}{12\mu} \quad (3)$$

with  $d_f$  as the fault aperture [L],  $\rho$  the density of water [ML<sup>-3</sup>],  $g$  the gravity acceleration [LT<sup>-2</sup>] and  $\mu$  the dynamic viscosity of water [MT<sup>-1</sup>L<sup>-1</sup>].

For groundwater flow in the karst conduits, the Manning equation was used (Eq. 4).

$$u_c = \frac{1}{n} \left( \frac{r_c}{2} \right)^{\frac{2}{3}} \sqrt{\frac{dH_c}{dx}} \quad (4)$$

9286

where  $u_c$  is the specific discharge in this case equaling the conduit flow velocity [ $L T^{-1}$ ],  $n$  is the Manning coefficient [ $T L^{-1/3}$ ],  $r_c/2$  the hydraulic radius [ $L$ ] and  $dH_c/dx$  the hydraulic gradient [-]. The Manning coefficient is an empirical value for the roughness of a pipe with no physical nor measurable meaning. The hydraulic radius is calculated

5 by dividing the cross-section by the wetted perimeter, which in this case corresponds to the total perimeter of the pipe (Reimann et al., 2011).  
The whole conduit network was simulated for turbulent flow conditions. Due to the large conduit diameters (0.01–6 m, Sect. 5) this assumption is a good enough approximation. Hereby, strong changes in flow velocities due to the change from laminar to

10 turbulent flow can be avoided. At the same time, the model does not require an estimation of the critical Reynold's number, which is difficult to assess accurately.  
The three-dimensional flow in the fissured matrix and the one-dimensional conduit flow were coupled through a linear exchange term that was defined after Barenblatt et al. (1960) as:

$$15 \quad q_{\text{ex}} = \frac{\alpha}{L}(H_c - H_m) \quad (5)$$

$q_{\text{ex}}$  is the water exchange between conduit and fissured matrix [ $L^2 T^{-1}$ ] per unit conduit length  $L$  [ $L$ ],  $H_m$  the hydraulic head in the fissured matrix [ $L$ ],  $H_c$  the hydraulic head in the conduit [ $L$ ] and  $\alpha$  the leakage coefficient [ $L^2 T^{-1}$ ]. The leakage coefficient was

$$20 \quad \alpha = 2\pi r_c K_m \quad (6)$$

with  $2\pi r_c$  as the conduit perimeter [ $L$ ]. Other possible influences e.g. the lower hydraulic conductivity at the solid-liquid interface of the pipe and the fact that water is not exchanged along the whole perimeter but only through the fissures are not considered.

25 The exact value of these influences is unknown and the exchange parameter mainly controls the reaction of the karst conduits and the fissured matrix to hydraulic impulses.  
Since the flow simulation is performed for steady-state conditions this simplification is not expected to exhibit significant influence on the flow field.

9287



## 2.2 Solute transport

Transient solute transport was simulated based on the steady-state groundwater flow field. Comsol Multiphysics® offers a general transport equation with its Solute Transport Interface. This interface was applied for the three-dimensional fissured matrix. In

5 this work saturated, conservative transport was simulated, which led to the following advection-dispersion equation for transport (Eq. 7):

$$\frac{\partial}{\partial t}(\theta_m c_m) + \nabla(\mathbf{u}_m c_m) = \nabla[(D_{Dm} + D_e)\nabla c_m] + S_m \quad (7)$$

10 with  $\theta_m$  being matrix porosity [-],  $c_m$  solute concentration [ $ML^{-3}$ ],  $D_{Dm}$  mechanical dispersion [ $L^2 T^{-1}$ ] and  $D_e$  molecular diffusion [ $L^2 T^{-1}$ ].  $S_m$  is the source term [ $L^3 T^{-1}$ ].

The Solute Transport Interface cannot be applied to one-dimensional elements within a three-dimensional model. Comsol® offers a so-called Coefficient Form Edge PDE Interface to define one-dimensional mathematical equations. There, a partial differential equation is provided (COMSOL AB, 2012) which can be adapted as needed and leads

15 to Eq. (8) in its application for solute transport in karst conduits:

$$\theta_c \frac{\partial c_c}{\partial t} + \nabla(-D_c \nabla c_c + u_c c_c) = f \quad (8)$$

The conduit porosity  $\theta_c$  is set equal to 1,  $D_c [L^2 T^{-1}]$  is the diffusive/dispersive term  $D_c = (D_{Dc} + D_e)$ ,  $f$  is the source term and  $u_c [L T^{-1}]$  is the flow velocity inside the conduits, which corresponds to the advective transport component. Flow divergence cannot be neglected, as is often the case in other studies (e.g. Hauns et al., 2001; Birk et al., 2006; Coronado et al., 2007). Different conduit sizes and in- and outflow along the conduits lead to significant velocity divergence in the conduits. If this is not considered there is no mass-conservation during the simulation. The mechanical conduit dispersion  $D_{Dc}$

$$25 \quad D_{Dc} = \varepsilon u_c \quad (9)$$

9288





the annual average ranging from  $0.068$  to  $0.135 \text{ m}^3 \text{ s}^{-1}$ . The fault zone aperture was calibrated accordingly (Sect. 5).

Due to a large number of studies conducted in the area during the last decades (e.g. Villinger, 1977; Sauter, 1992; Geyer et al., 2008; Kordilla et al., 2012; Mohrlök, 2014) many data for pattern matching are available even though the karst conduit network itself is not accessible. Since the groundwater flow simulation was performed for steady-state conditions, direct recharge, which is believed to play an important role during event discharge (Geyer et al., 2008), was neglected. **It is not expected to exhibit significant influence on the steady-state flow field.** From Sauter (1992) the long-term average annual recharge, ranges of hydraulic parameters and the average annual hydraulic head distribution derived from 20 observation wells (Fig. 1) are available. Villinger (1993) and Sauter (1992) provided data on the geometry of the aquifer base.

Geyer et al. (2008) calculated the maximum conduit volume for the Gallusquelle spring  $V_c [\text{L}^3]$  with information from the tracer test that will be referred to as tracer test 2 in the following. Since the injection point of the tracer test is close to the catchment boundary, it is assumed that it covers the whole length of the conduit system. Assuming a relationship after Eq. (13) the authors calculated the maximum volume at  $218\,000 \text{ m}^3$ .

$$V_c = Q_s t_m \quad (13)$$

$Q_s [\text{L}^3 \text{ T}^{-1}]$  is the spring discharge and  $t_m [\text{T}]$  the mean tracer travel time. The approach assumes the volume of the conduit corresponds to the total volume of water discharged during the time between tracer input and tracer arrival neglecting the contribution of the fissured matrix.

The six springs that were observed and therefore simulated are shown in Fig. 1. Except for the Balinger Quelle spring, their discharges were fitted to long-term average annual discharge data. For the Balinger Quelle spring discharge calibration was not possible due to lack of data. It was included as a boundary condition because several tracer tests provided a valuable basis for the conduit structure leading to the spring. The Gallusquelle spring is the largest and best investigated spring in the area. Therefore,

9291

parameters were first calibrated for the Gallusquelle spring to fit the spring discharge within the range of  $10 \text{ L s}^{-1}$  and afterwards the discharge of the other springs was examined.

Tracer directions were available for 32 tracer tests conducted at 20 different tracer injection locations (Oehlmann et al., 2013). 16 of the tracer tests were registered at the Gallusquelle spring. For this work two of them were chosen for pattern matching of transport parameters. Both of them were assumed to have a good and direct connection to the conduit network. Tracer test 1 (Geyer et al., 2007) has a tracer injection point at a distance of three kilometres to the Gallusquelle spring. Tracer test 2 (MV746 in Merkel, 1991; Reiber et al., 2010) was conducted at 10 km distance to the Gallusquelle spring (Fig. 1). Due to the flow conditions (Fig. 1) it can be assumed that tracer test 2 covers the total length of the conduit network feeding the Gallusquelle spring. The recovered tracer mass was chosen as input for the tracer test simulation. The basic information about the tracer tests is given in Table 1.

**Since the tracer tests were not performed at average flow conditions, the model parameters were calibrated first for the long-term average annual recharge of  $1 \text{ mm d}^{-1}$  and the long-term average annual discharge of  $0.5 \text{ m}^3 \text{ s}^{-1}$ .** For the transport simulations, the recharge was then adapted to produce the respective discharge observed during the tracer experiment (Table 1).

#### 4 Parameter analysis

**An extensive parameter analysis was performed in order to identify the most important parameters and factors as well as their relative contributions to the discharge and conduit flow velocities.** The five basic scenarios are summarized in Fig. 2 and Table 2. They analyse different variations of hydraulic parameters of the fissured matrix and karst conduits as well as variations in conduit geometry. Reproducing the discharge of the Gallusquelle spring was the basic requirement for a simulation to be taken into account. **Each scenario is based on the scenario before that shows the best fit.** If no

9292





difference in model quality could be observed, the simpler model is chosen as a basis for further simulations. The fit of the tracer tests is determined by comparing the arrival times of the highest peak concentration of the simulation with the measured value (peak-offset). Since tracer experiments conducted in karst conduits usually display very narrow breakthrough curves, this procedure appears to be justified.

#### 4.1 Scenario 1 – standard scenario

In scenario 1 all features were implemented as described in Sects. 2 and 3. Different conduit geometries were tested. They were defined by their smallest conduit radii  $b$  and their slopes of radius increase along the conduit length  $m$  (Eq. 1). For each geometry only one value of the Manning coefficient  $n$  allows a simulated discharge for the Gallusquelle spring of  $0.5 \text{ m}^3 \text{ s}^{-1}$ . The  $n$  value correlates well with that for the total conduit volume due to the fact that the spring discharge is predominantly determined by the transmissivity of the karst conduit system. The transmissivity of the conduit system at each point in space is the product of its hydraulic conductivity, which is proportional to  $1/n$ , and the cross-sectional area of the conduit  $A$ . Thus, higher conduit areas go along with higher  $n$  values and vice versa.

The observed hydraulic gradients in the Gallusquelle area are not uniform along the catchment. Figure 3 shows a S-shaped distribution with distance to the Gallusquelle spring. This shape results from the combination of the respective transmissivity at each point of the area and total flow. The amount of water flowing through a cross-sectional area increases towards the springs due to flow convergence. In the Gallusquelle area, the transmissivity rises in the vicinity of the springs leading to a low hydraulic gradient. In the central part of the area discharge is relatively high while the transmissivities are lower leading to the observed steepening of the gradient starting in a distance of 4000 m to 5000 m from the Gallusquelle spring. Towards the boundary of the catchment area in the West the water divide reduces discharge in the direction of the Gallusquelle spring leading to a smoothing of hydraulic gradients.

9293



With scenario 1 it is possible to achieve a hydraulic head fit resulting in a root mean square error (RMSE) of 6 m that can be judged as adequate on catchment scale. A good fit can be achieved with small  $b$  values independently of the chosen  $m$  value (Fig. 3a). This means that the hydraulic head fit is independent of the conduit volume. The higher the  $b$  value, the higher the  $m$  value has to be to reproduce the hydraulic gradients of the area (Fig. 3). There are several parameter combinations providing a good fit for the Gallusquelle spring discharge and the hydraulic head distribution.

The parameter analysis shows that it is possible to simulate only either of the tracer tests with this scenario (Fig. 4). Given the broad range of geometries for which an adequate hydraulic head fit can be achieved (Fig. 3) it is possible to simulate one of the two tracer peak velocities and the hydraulic head distribution with the same set of parameters. While tracer test 1 needs relatively high  $n$  values, of about  $2.5 \text{ s m}^{-1/3}$ , tracer test 2 can only be calibrated with lower values of about  $1.7 \text{ s m}^{-1/3}$  (cf. Fig. 4a and b). For every parameter set, where the simulated tracer test 2 is not too slow, tracer test 1 is much too fast. For simulating tracer test 2, the velocities at the beginning of the conduits must be relatively high. To avoid the flow velocities getting too high downgradient the conduit size would have to increase drastically due to the constant additional influx of water from the fissured matrix. In the given geometric range, the conduit system has a dominant influence on spring discharge. Physically, this situation corresponds to the conduit-influenced flow conditions (Kovács et al., 2005). Thus, conduit transmissivity is a limiting factor for conduit-matrix exchange and a positive feedback mechanism is triggered, if the conduit size is increased. A higher conduit size leads to higher groundwater influx from the fissured matrix and spring discharge is overestimated. Therefore, parameter analysis shows that scenario 1 is too strongly simplified to correctly reproduce the complex nature of the aquifer.

9294

## 4.2 Scenario 2 – conduit roughness coefficient $K_c$

In scenario 2 the Manning coefficient  $n$  was changed from constant to laterally variable. In the literature,  $n$  is generally kept constant throughout the conduit network (e.g. Jeannin, 2001; Reimann et al., 2011) for lack of information on conduit geometry. However the Gallusquelle is not a single large spring fed by one pipe, but consists of several small outlets across a certain discharge area fed by a bundle of relatively small, interacting pipes.

Therefore, it can be assumed that the increase in conduit cross-section is at least partly provided by additional conduits added to the bundle rather than a single individual widening conduit. While the flow cross-section gradually grows with time, the surface-volume-ratio increases as well leading to a higher roughness, further enhanced by exchange processes between the individual conduits. This would lead to an increase of the Manning coefficient towards the spring for a simulated single conduit. Since the number and size of the conduits is unknown, it is impossible to calculate the change of  $n$  directly from the geometry. Thus, a simple scenario was assumed where the roughness coefficient  $K_c$ , which is the reciprocal of  $n$ , was linearly and negatively coupled to the rising conduit radius (Eq. 14).

$$K_c = \frac{1}{n} = -m_h r_c + m_h r_{c,max} + b_h \quad (14)$$

with  $r_c$  [L] as the conduit radius and  $r_{c,max}$  [L] as the maximum conduit radius simulated for the respective spring, which Comsol<sup>®</sup> calculates from Eq. (1).  $m_h$  [-] and  $b_h$  [L] are calibration parameters determining the slope and the lowest value of the roughness coefficient respectively.

For every conduit geometry several combinations of  $m_h$  and  $b_h$  lead to the same spring discharge. However, hydraulic head fit and tracer velocities are different for each  $m_h$ – $b_h$  combination even if spring discharge is the same. With the new parameters a higher variation of velocity profiles is possible. This allows for the calibration of the tracer velocities of both tracer tests. The dependence of tracer test 2 on  $m_h$  is much

9295

higher than that of tracer test 1 since it is injected much further upgradient towards the beginning of the conduit (Fig. 5). Therefore, tracer test 2 benefits more strongly from the higher velocities far away from the spring introduced by high  $m_h$  values and always shows a significant positive correlation with  $m_h$  (Fig. 5).

Since the slope of  $K_c$  is negative with respect to the conduit length, the variable  $K_c$  leads to a slowing down of water towards the springs. As discussed in detail by Oehlmann et al. (2013) a rise of transmissivity towards the springs is observed in the Gallusquelle area. Therefore, adequate hydraulic head fits can only be obtained, if the decrease of  $K_c$  towards the spring is not too large and compensates the effect of the increase in conduit transmissivity due to the increasing conduit radius. This effect reduces the number of possible and plausible parameter combinations. From these considerations a best-fit model can be deduced capable of reproducing all important parameters within an acceptable error range. According to the model simulations, karst groundwater discharge and flow velocities significantly depend on the total conduit volume as is to be expected. It can be deduced from the parameter analysis that the conduit volume can be estimated at ca. 100 000 m<sup>3</sup> for the different parameters to match equally well (Fig. 6a).

## 4.3 Scenario 3 – extent of conduit network

In scenario 3, a laterally further extended conduit system was employed, assuming the same maximum conduit volume as in scenarios 1 and 2 but with different spatial distribution along the different total conduit lengths. The original conduit length for the Gallusquelle spring in scenarios 1 and 2 is 39 410 m, for scenario 3 it is 63 490 m, so the total length was assumed to be larger by ca. 50% (Fig. 7). The geometry of the original network was mainly constructed based on qualitative evaluation from artificial tracer tests, where point-to-point connections are observed. Therefore, it represents the minimal extent of the conduit network. For scenario 3 the network was extended along dry valleys, where no tracer tests were conducted.



The results of the parameter variations are comparable to those of scenario 2 (cf. Fig. 6a and b). While the hydraulic head contour lines are smoother than for the original conduit length the general hydraulic head fit is the same (Fig. 6b). It seems possible to obtain a good fit for all model parameters but the scenario is more difficult to handle numerically. Calculation times are up to ten times larger compared to the other scenarios and goodness of convergence is generally lower. Since the calibrated parameters are not significantly different from those deduced in scenario 2 it is concluded that the ambiguity introduced by the uncertainty in total conduit length is small if hydraulic conduit parameters and total conduit volumes are the aim of investigation.

#### 10 4.4 Scenario 4 – matrix hydraulic conductivity $K_m$



In scenario 4, the homogeneously chosen hydraulic conductivity of the fissured matrix  $K_m$  was changed into a laterally variable conductivity based on different types of lithology and the spatial distribution of the groundwater potential. Sauter (1992) found from field measurements that the area can be divided into three parts with different hydraulic conductivities. Oehlmann et al. (2013) discussed that the major influence is the conduit geometry leading to higher hydraulic transmissivities close to the springs in the East of the area. It is also possible that not only the conduit diameters change towards the spring but the hydraulic conductivity of the fissured matrix as well, since the aquifer cuts through three stratigraphic units (Sect. 3). These geologic changes are likely to affect the lateral distribution of hydraulic conductivities (Sauter, 1992). Figure 8 shows the division into three different areas.  $K_m$  values were varied in the range of the values measured by Sauter (1992).

The influence of the hydraulic conductivity of the fissured matrix  $K_m$  on flow velocities inside the karst conduits is comparatively small and decreases further in the vicinity of the springs leading to minor influences on tracer travel times. It was expected that a laterally variable  $K_m$  value has a major influence on the hydraulic head distribution. All variations of scenario 2 that produce good results for both tracer tests and have a high total conduit volume above 100 000 m<sup>3</sup> yield poor results for hydraulic head errors and

9297

spatial distributions of the hydraulic heads (Fig. 6a). For scenario 4, two different conduit configurations (geometries) were chosen that achieve good results with respect to conduit flow velocities. Geometry G1 has a conduit volume of 112 000 m<sup>3</sup>. G2 has a higher  $b$  value which leads to the maximum conduit volume of ca. 150 000 m<sup>3</sup>. All parameters for the two simulations are given in Table 3.

It was found that while the maximum root mean square error of the hydraulic head fit is similar for both geometries, the minimum RMSE for the hydraulic head is determined by the conduit system. It is not possible to compensate an unsuitable conduit geometry with suitable  $K_m$  values (Fig. 6c), which assists in the independent conduit network and fissured matrix calibration. This observation increases the confidence in the representation of the conduits and improves the possibility to deduce the conduit geometry from field measurements. For a well-chosen conduit geometry, laterally variable matrix conductivities do not yield any improvement. The approach introduces additional parameters and uncertainties because the division of the area into three parts is not necessarily obvious without detailed investigation. From the distribution of the exploration and observation wells (Fig. 1) it is apparent that especially in the South and West the boundaries are not well defined.



#### 15 4.5 Scenario 5 – conduit intersections

In scenario 5, the effect of the conduit diameter change at intersections was investigated. In the first four scenarios the possible increase in cross-sectional area at intersecting conduits was neglected. In nature however, the influx of water from another conduit is likely to influence conduit evolution and therefore its diameter. In general, higher flow rates lead to increased dissolution rates because dissolution products are quickly removed from the reactive interface, especially if conditions are turbulent (Clemens, 1998) and no diffusion dominated layer limits the overall dissolution process. Clemens (1998) simulated karst evolution in simple Y-shaped conduit networks and found higher diameters for the downstream conduit even after short simulation times. Preferential conduit widening at intersections could further be enhanced by the process of mixing

9298

corrosion (Dreybrodt, 1981). Hückinghaus (1998) found during his karst network evolution simulations that the water from other karst conduits has a very high saturation with respect to  $\text{Ca}^{2+}$  compared to water entering the system through direct recharge. Thus, if direct recharge is present, the mixing with nearly saturated water from an intersecting conduit could hamper the evolution of the conduit downstream. In Hückinghaus' (1998) simulation this effect led to abandonment of a flow path that had more neighboring conduits for a flow path with fewer. This could further slow down the preferential evolution of downstream conduits. In scenario 5 the influence of the increase in diameter due to the above processes was investigated, i.e. the cross-sections of two intersecting conduits were added and used as starting cross-section for the downstream conduit. The new conduit radius was then calculated after Eq. (15) at each intersection.

$$r_{c2} = \sqrt{r_{c0}^2 + r_{c1}^2} \quad (15)$$

with  $r_{c2}$  being the conduit radius downstream of the intersection and  $r_{c0}$  and  $r_{c1}$  the conduit radii of the two respective conduits before their intersection.

Results are very similar to those of scenario 2 (cf. Fig. 6a and d). Both simulations result in nearly the same set of parameters (Table 4). The estimated conduit volume is even a little smaller for scenario 5 since larger cross-sections in the last conduit segment near the spring are reached for a lower total conduit volume. The drastic increase of conduit cross-sections at the network intersections leads to higher variability in the cross-sections along the conduit segments. The differences between the peak-offsets of both tracer tests are very high compared to those of scenario 2. While the peak time of tracer test 2 can be calibrated for large conduit volumes, i.e. conduit volumes above  $120\,000\text{ m}^3$ , (Fig. 6d) the peak time of tracer test 1 is too late for large conduit volumes. This is due to the fact that the injection point for tracer test 1 is much closer to the spring than that for tracer test 2. In scenario 5 the conduit volume is spatially differently distributed from that of scenario 2 for the identical total conduit volume. The drastic increase in conduit diameters downgradient of conduit intersections leads to rather high conduit diameters in the vicinity of the spring. Therefore, while tracer transport in tracer

9299

test 2 occurs in relatively small conduits with high velocities and larger conduits with lower flow velocities, the tracer in tracer test 1 is only transported through the larger conduits whose flow velocities are restricted by the spring discharge. In Fig. 6d the parameter values for the best fit would lie well below the lower boundary of the diagram at negative values below  $-10\text{ h}$ . Since the fit for conduit volumes around  $100\,000\text{ m}^3$  is similar to that of scenario 2, however, the two scenarios can in this case not be distinguished based on field observations.

## 5 Discussion

The parameter analysis shows that there is only a limited choice of parameters with which the spring discharges, the hydraulic head distribution and the tracer velocities can be simulated. Scenario 1 is the only scenario that cannot reproduce the peak travel times observed in both tracer tests simultaneously (Sect. 4.1). Scenarios 3 and 4 only make the model more complex without significant model improvement. They do not show any advantage compared to scenario 2 and are therefore not considered further. Scenarios 2 and 5 are both judged suitable. Their parameters and the quality of the fit are similar. The numerical effort for both scenarios is equivalent. Scenario 5 has an additional term in the calculation of the conduit radius whereas flow velocities in scenario 2 might increase abruptly at the intersections, which can lead to numerical problems for coarser meshes. Table 4 summarizes all parameters for both simulations and Fig. 9 shows the simulated tracer breakthrough curves and spring discharges.

### 5.1 Final model calibration

The main objective of the model simulation is not only to reproduce the target values but to also provide insight into dominating flow and transport processes, sensitive parameters and to check the plausibility of the model set-up. Furthermore, the predictive power of the model is being examined i.e. the response of model output to a variation in

hydraulic transport parameters and model geometries. Possible ambiguities in parameterizations can also be caused, i.e. different combinations of parameters producing identical model output.

For these aims model parameters and aquifer properties simulated with scenarios 2 and 5 are compared to those observed in the field. As apparent from Table 4 most of the calibrated parameters range well within values provided in the literature. The calibrated Manning coefficients are relatively high compared to other karst systems. Jeannin (2001) lists effective conductivities for several different karst networks that translate into  $n$  values of between 0.03 and  $1.07 \text{ s m}^{-1/3}$ , showing that the natural range of  $n$  values easily extends across two orders of magnitude and the minimum  $n$  values of the simulation lie within the natural range. The maximum  $n$  values are significantly higher than those given by Jeannin (2001). This is not surprising since usually  $n$  values are given for single pipes. The maximum  $n$  values of the simulation refer to a bundle of small diameter conduits simulated as a single pipe, i.e. roughness is significantly enhanced. The high calibrated  $n$  values thus result from the modelling approach of simplified representation of the conduit system with straight large pipes. The large-scale simulation approach for the whole catchment area prevents the simulation of small individual conduits resulting in a calibrated  $n$  value that includes geometric conduit properties in addition to the wall roughness that it was originally defined for. This effect is specific for the Gallusquelle area but it might be important to consider for other moderately karstified areas as well where identification of conduit geometries is especially difficult.

Deviations from literature values can be observed for the total conduit volume for the Gallusquelle spring as well. Both simulations yield conduit volumes of ca.  $100\,000 \text{ m}^3$ . The estimation with traditional methods based on a single tracer experiment overestimates the conduit volume by up to 100 % because the matrix contribution is neglected. Since the conduit transmissivity increases towards the spring water enters the conduits preferably in the vicinity of the spring in the Gallusquelle area. Therefore, the matrix contribution is high. In addition, the travel time at peak concentration of tracer test 2 is longer than three days, during which time matrix-conduit water exchange can

9301

readily take place. Based on the results of a tracer test conducted in a distance of 3 km to the Gallusquelle spring Birk et al. (2005) estimated the error incurred by deducing the conduit volume without taking conduit-matrix exchange fluxes into account with a very simple numerical model. The authors found a difference in conduit volumes of approximately 50 %. This fits well with the results of this simulation.

The value for the conduit cross-section  $A$  at the Gallusquelle spring lies higher than the representative conduit diameters calculated by Birk et al. (2005). The author derived a diameter of ca. 4.2 m, which corresponds to a cross-sectional area of  $13.9 \text{ m}^2$ , while the simulated cross-section at the spring is about  $20 \text{ m}^2$  for scenarios 2 and 5 (Table 4). However, the value of Birk et al. (2005) is representative for the whole conduit system between their tracer injection point and the spring. The average cross-section between these two points is  $11.9 \text{ m}^2$  for scenario 2 and  $13.4 \text{ m}^2$  for scenario 5, which fits very well to the results of Birk et al. (2005).

The quality of the simulation of tracer breakthrough was estimated based on the difference between measured and simulated peak concentration times (peak-offset). The quality of the fit was judged as satisfactory if the peak-offset was lower than either the simulation interval or the measurement interval in the field. Time differences lower than these intervals are negligible since they are smaller than the overall temporal resolution of the breakthrough curve. This criterion was reached for both tracer tests for scenarios 2 and 5. It was not possible to match the shape of both breakthrough curves with the same dispersivity. The apparent dispersion in the tracer test 2 breakthrough is much higher than that of tracer test 1, while tracer test 1 shows a more expressed tailing (Fig. 9a and b). This corresponds to the effect observed by Hauns et al. (2001). The authors found scaling effects in karst conduits: the larger the distance between input and observation point, the more mixing occurred. The tailing is generally induced by matrix diffusion or discrete geometric changes such as pools, where the tracer can be held back and released more slowly. Theoretically, every water drop employs medium and slow flow paths if the distance is large enough, leading to a more or less symmetrical, but broader, distribution and therefore a higher apparent dispersion (Hauns et al.,

9302

2001). To quantify this effect, exact knowledge of the geometric conduit shape such as the positions and shapes of pools would be necessary. Furthermore, an additional unknown possibly influencing the observed retardation and dispersion effects is the input mechanism. The simulation assumes that all introduced tracer immediately and completely enters the conduit system, which neglects effects of the unsaturated zone on tracer breakthrough curves. In addition, the shape of the breakthrough curve of tracer test 2 is difficult to deduce since the six hours sampling interval can be considered as rather low leading to a breakthrough peak which is described by only seven measurement points. The concentrations between those points are unknown and the maximum concentration might be higher than the measured maximum, if it was reached between measurements. Therefore, dispersivity was calibrated for both breakthrough curves separately. Calibrated dispersivity ranges well within those quoted in literature (Table 4). The mass recovery during the simulation was determined to range between 98.4 % and 99.9 % in all simulations. The slight mass difference results from a combination of diffusion of the tracer into the fissured matrix and numerical inaccuracies.

The spring discharge was calibrated for the Gallusquelle spring and the other springs were simulated with the same parameters. In most cases this leads to a slight underestimation of spring discharge (Fig. 9c). For the smaller springs the models of scenarios 2 and 5 provide similar results. The underestimation of discharge is in the order of  $< 0.05 \text{ m}^3 \text{ s}^{-1}$  and is not expected to significantly influence the general flow conditions. It probably results from the unknown conduit geometry in the catchments of the different minor springs. It was assumed that all springs show the same type of conduit bundles as the Gallusquelle spring but this assumption cannot be confirmed. The only case in which the two scenarios give significantly different results is the spring discharge of the spring group consisting of the Ahlenberg- and Büttнауquellen springs (Fig. 9c). Scenario 2 overestimates and scenario 5 underestimates the discharge. This is due to the fact that the longest conduit of the Ahlenberg- and Büttнауquellen springs is longer than the longest one of the Gallusquelle spring but the conduit network has less intersections (Fig. 1). Therefore the conduit volume of the Ahlenberg- and Büttнауquellen

9303

springs is  $134\,568 \text{ m}^3$  in scenario 2 and only  $75\,085 \text{ m}^3$  in scenario 5 leading to the different discharge values. It is reasonable to assume that a better fit for the spring group can be achieved, if more variations of conduit intersections are tested. An adequate fit for the Fehla-Ursprung spring of  $0.1 \text{ m}^3 \text{ s}^{-1}$  was achieved for both scenarios with a fault aperture of 0.005 m.

The most important uncertainties regarding the reliability of the simulation include the assumptions that were made prior to modelling. First, flow dynamics were neglected. This approach was chosen because tracer tests are supposed to be conducted during quasi-steady state flow conditions. However, this is only the ideal case. During both tracer tests spring discharge declined slightly. The influence of transient flow on transport velocities inside the conduits was estimated by a very simple transient flow simulation for the best-fit models in which recharge and storage coefficients were calibrated to reproduce the observed decline in spring discharges. The transient flow only slightly affected peak velocities but lead to a larger spreading of the breakthrough curves and therefore lower calibrated dispersion coefficients. This effect occurred because the decline in flow velocities is not completely uniform inside the conduits and depending on where the tracer is at which time it experiences different flow velocities in the different parts of the conduits, which leads to a broader distribution at the spring. The same breakthrough curves can be simulated under steady-state flow conditions with slightly higher dispersivity coefficients. So, the calibrated dispersivities do not only represent geometrical heterogeneities but also temporal as is the case for all standard evaluations of dispersion from tracer breakthrough curves.

Furthermore, flow in all karst conduits was simulated for turbulent conditions. Turbulent conditions can be generally assumed in karst conduits (Reimann et al., 2011) and also apply to all calibrated model conduit cross-sections. Since the conduit cross-section presents the total cross-section of the conduit bundle, the cross-sections of the individual tubes are uncertain, though. The high roughness  $n$  values suggest that the surface/volume ratio is relatively high, which implies that the individual conduit cross-sections are rather small. Therefore, laminar flow in some conduits is likely. While

9304

laminar flow conditions in the conduits influence hydraulic gradients considerably, this fact is believed not to influence the overall results and conclusions of this study, i.e. the relative significance of the parameters deduced from parameter analysis and the deduced conduit volume, especially since flow is simulated for steady-state conditions.

## 5.2 Calibration strategy

For a successful calibration of a groundwater flow and transport model for a karst area on catchment scale certain constraints have to be set a priori. The geometry of the model area, i.e. locations/types of boundary conditions and aquifer base, fixed during calibration, has to be known with sufficient certainty. Furthermore, the objective functions for calibration have to be defined, i.e. the hydraulic response of the system and transport velocities. In a karst groundwater model, these consist of measurable variables, i.e. spring discharges, hydraulic heads in the fissured matrix and two tracer breakthrough curves. The hydraulic head measurements should be distributed across the entire catchment and preferably close to the conduit system, should geometric conduit parameters be calibrated for as well. It is expected that the influence of the conduits on the hydraulic head decreases and the influence of matrix hydraulic conductivities increases with distance to the conduit system. In the design of the tracer experiment, the following criteria should be observed: for a representative calibration, the dye should be injected at as large a distance to each other as possible with one of them including the length of the whole conduit system. Each tracer test gives integrated information about its complete flow path. If the injection points lie close together, no information about the development of conduit geometries from water divide to spring can be obtained. Further, the dye should be injected as directly as possible into the conduit system, e.g. via a flushed sinkhole, to obtain information on the conduit flow regime and to minimize matrix interference. To ease interpretation a constant spring discharge during the tests is desirable.

In this study, the flow field was not only simulated for the catchment area of the Gallusquelle spring, but for a larger area including the catchment areas of several smaller

9305

springs (Fig. 1). This is in general not essential for deducing conduit volumes and setting up a flow and transport model. Simulating several catchments helps to increase the reliability of the simulation, however. The positions of water divides are majorly determined by the hydraulic conductivity of the fissured matrix  $K_m$ , so that the simulated catchment areas of the different springs can be used to estimate how realistic the simulated flow field is and decrease the range of likely  $K_m$  values. In this study, high  $K_m$  values above ca.  $3 \times 10^{-5} \text{ m s}^{-1}$  made the simulation of the spring discharge of the Fehla-Ursprung spring (Fig. 1) impossible because the water divide in the West could not be simulated and most of the water in the area discharged to the East towards the river Lauchert resulting in a very narrow and long catchment area for the Gallusquelle spring.

There are eight parameters available for model calibration in this study. Two of these parameters define the conduit geometry:  $b$  is the lowest conduit radius and  $m$  the slope with which the conduit radius increases. One parameter,  $d_f$ , defines the aperture of the fault zone. The hydraulic conductivity of the fissured matrix is represented by the parameter  $K_m$  and the roughness of the conduit system by two parameters:  $b_h$  represents the highest roughness and  $m_h$  the slope of roughness decrease in upgradient direction from the spring. The last two parameters  $\varepsilon_1$  and  $\varepsilon_2$  are the respective conduit dispersivities obtained from the two tracer experiments.

For efficiency reasons it is important to know which of these parameters can be calibrated independently. The apparent transport dispersivities  $\varepsilon_1$  and  $\varepsilon_2$  are pure transport parameters, which influence only the shape of the breakthrough curves and not the flow field. In this study they were calibrated separately after calibration for hydraulic and geometric parameters.

Only for hydraulically dominant fault zones knowledge of the fault zone aperture  $d_f$  is required. For the model area this parameter was required for one fault zone lying in the West of the area feeding the Fehla-Ursprung spring (Fig. 1). Since the Fehla-Ursprung spring has its own catchment area the fault zone has only minor influence on the flow regime in the Gallusquelle catchment. Its hydraulic parameters were calibrated at the

9306





beginning of the simulation procedure to reproduce the catchment and the discharge of the Fehla-Ursprung spring adequately and kept constant throughout all the simulations. In the final calibrated models it was rechecked, but the calibrated value was still acceptable.

5 The hydraulic conductivity of the fissured matrix  $K_m$  can be calibrated independently in principle as well. The influence on spring discharge is relatively small. The best-fit  $K_m$  value depends on the conduit parameters, i.e. geometry and roughness, since the hydraulic conductivities of the conduit system and of the fissured matrix define the total transmissivity of the catchment area together. Nonetheless, the best-fit value lies in  
10 the same range for different conduit geometries (cf. Fig. 6c). The greater the difference between the simulated conduit geometries, the more likely is a slight shift of the best-fit  $K_m$  value. Therefore, it is advisable to calibrate it anew for significant model changes, e.g. different scenarios, but to keep it constant during the rest of the calibrations. For the best-fit configuration, potentially used as a prognostic tool, the  $K_m$  value needs to be  
15 checked and adapted if necessary. This observation is, however, only valid for steady-state flow conditions. The dynamics of the hydraulic head and spring discharge might be highly sensitive to the matrix hydraulic conductivity, the conduit-matrix exchange coefficient and the lateral conduit extent. This work focuses on the conduits as highly conductive pathways for e.g. contaminant transport, but the calibration of matrix velocities, e.g. by use of environmental tracers, would likely be sensitive to the  $K_m$  values as well.

The conduit parameters for geometry and roughness, here four parameters (lowest conduit radius  $b$ , slope of radius increase  $m$ , lowest roughness coefficient/highest roughness  $b_h$  and slope of roughness decrease  $m_h$ ), have to be varied simultaneously.  
25 All of them have a major influence on spring discharge and cannot be varied separately without introducing discharge errors. For each conduit geometry, there are a number of possible  $b_h$ - $m_h$  combinations that result in the observed spring discharge. In general, the slowest transport velocities are achieved with a  $m_h$  value of zero. So, to deduce the range of geometric parameters that reproduce the objective functions, it is advisable to

9307

check the minimum conduit volume for which the tracer tests are not too fast for a value of  $m_h$  equal to zero. For the Gallusquelle area, transmissivities significantly increase towards the springs, which is characteristic for most karst catchments. Therefore low  $b_h$  values oppose the general hydraulic head trend: they increase the conduit roughness at the spring leading to slower flow and higher gradients. The higher the conduit  
5 volume, the higher  $b_h$  is required to reproduce the observed transport velocities. Therefore, the best-fit model likely has the smallest conduit volume for which both tracer tests can be reproduced. In Fig. 6 this condition can be seen to clearly range in the order of  $100\,000\text{ m}^3$  for the Gallusquelle area. While the four conduit parameters allow for  
10 a good model fit, they are pure calibration parameters. They show that the karst conduit system has a high complexity, which cannot be neglected. A systematic simulation of the heterogeneities, e.g. with a karst genesis approach, would be a process-based improvement to the current method and give more physical meaning to the parameters.

## 6 Conclusions

15 The study presents a large-scale catchment based hybrid karst groundwater flow model capable of simulating groundwater flow *and* solute transport. For average flow conditions this model can be used as a predictive tool for the Gallusquelle area with relative confidence. The approach of simultaneous pattern matching of flow and transport parameters provides new insight into the hydraulics of the Gallusquelle conduit system.  
20 The model ambiguity was significantly reduced to the point where an estimation of the actual karst conduit volume for the Gallusquelle spring could be made. This would not have been possible simulating only one or two of the three objective functions, i.e. the hydraulic head distribution and two tracer tests. Standard methods employing only one tracer test for the estimation of conduit volumes can only approximate the maximum  
25 volume.

The model allows the identification of the relevant parameters and factors affecting karst groundwater discharge and transport in karst conduits and the examination of

9308



the respective overall importance in a well-investigated karst groundwater basin. While a differentiated representation of the roughness values in the karst conduits is substantial for buffering the lack of knowledge of the exact conduit geometry, e.g. local variations in cross-section and the amount of interacting conduits, variable matrix hydraulic conductivities cannot improve the simulation. It was shown that the effect of the unknown exact lateral extent of the conduit system and the change in conduit cross-section at conduit intersections is of minor importance for the overall karst groundwater discharge. This is important since these parameters are usually unknown and difficult to measure in the field.

For calibration purposes, this study demonstrates that for a steady-state flow field the hydraulic conductivities of the fissured matrix can practically be calibrated independently of the conduit parameters. Furthermore, a strategy for the simultaneous calibration of conduit volumes and conduit roughness in a complex karst catchment was developed.

As discussed in Sect. 5 the major limitation of the simulation is the neglect of flow dynamics. Therefore, transient flow simulation is the focus of ongoing work. This will extend the applicability of the model as a prognostic tool to all essential field conditions and lead to further conclusions regarding the important karst system parameters, their influences on karst hydraulics and their interdependencies. It can be expected that some parameters, which are of minor importance in a steady-state flow field, e.g. the lateral conduit extent and the percentage of recharge entering the conduits directly, will exhibit significant influence for transient flow conditions.

*Acknowledgements.* The presented study was funded by the German Federal Ministry of Education and Research (promotional reference No. 02WRS1277A, AGRO, “Risikomanagement von Spurenstoffen und Krankheitserregern in ländlichen Karsteinzugsgebieten”).

This Open Access Publication is funded by the University of Göttingen.

9309

## References

- Barenblatt, G. I., Zheltov, I. P., and Kochina, I. N.: Basic concepts in the theory of seepage in fissured rocks (strata), *J. Appl. Math. Mech.-USSR*, 24, 1286–1303, 1960 (English translation).
- Bauer, S., Liedl, R., and Sauter, M.: Modeling of karst aquifer genesis: Influence of exchange flow, *Water Resour. Res.*, 39, 1285, doi:10.1029/2003WR002218, 2003.
- Birk, S., Geyer, T., Liedl, R., and Sauter, M.: Process-based interpretation of tracer tests in carbonate aquifers, *Ground Water*, 43, 381–388, 2005.
- Birk, S., Liedl, R., and Sauter, M.: Karst spring responses examined by process-based modeling, *Ground Water*, 44, 832–836, 2006.
- Clemens, T.: Simulation der Entwicklung von Karstaquiferen, Ph.D. thesis, Eberhard-Karls-Universität zu Tübingen, Tübingen, 1998.
- Clemens, T., Hückinghaus, D., Sauter, M., Liedl, R., and Teutsch, G.: A combined continuum and discrete network reactive transport model for the simulation of karst development, in: Proceedings of the ModelCARE 96 Conference, 24–26 September 1996, Golden, Colorado, USA, 237, 1996.
- COMSOL AB: COMSOL Multiphysics® User’s Guide v4.3, 1292 pp., 2012.
- Coronado, M., Ramírez-Sabag, J., and Valdiviezo-Mijangos, O.: On the boundary conditions in tracer transport models for fractured porous underground formations, *Rev. Mex. Fís.*, 53, 260–269, 2007.
- Doummar, J., Sauter, M., and Geyer, T.: Simulation of flow processes in a large scale karst system with an integrated catchment model (Mike She) – Identification of relevant parameters influencing spring discharge, *J. Hydrol.*, 426, 112–123, doi:10.1016/j.jhydrol.2012.01.021, 2012.
- Dreybrodt, W.: Mixing in  $\text{CaCO}_3$ – $\text{CO}_2$ – $\text{H}_2\text{O}$  systems and its role in the karstification of limestone areas, *Chem. Geol.*, 32, 221–236, 1981.
- Ford, D. C. and Williams, P. W.: *Karst Geomorphology and Hydrology*, Wiley, West Sussex, 562 pp., 2007.
- Geyer, T., Birk, S., Licha, T., Liedl, R., and Sauter, M.: Multi-tracer test approach to characterize reactive transport in karst aquifers, *Ground Water*, 45, 36–45, 2007.
- Geyer, T., Birk, S., Liedl, R., and Sauter, M.: Quantification of temporal distribution of recharge in karst systems from spring hydrographs, *J. Hydrol.*, 348, 452–463, 2008.

9310



- Golwer, A.: Erläuterungen zu Blatt 7821 Veringenstadt, Geologische Karte 1 : 25 000 von Baden-Württemberg, Geologisches Landesamt Baden-Württemberg, Stuttgart, 151 pp., 1978.
- Gwinner, M. P.: Erläuterungen zu Blatt 7721 Gammertingen, Geologische Karte 1 : 25 000 von Baden-Württemberg, Geologisches Landesamt Baden-Württemberg, Freiburg/Stuttgart, 78 pp., 1993.
- Hauns, M., Jeannin, P.-Y., and Atteia, O.: Dispersion, retardation and scale effect in tracer breakthrough curves in karst conduits, *J. Hydrol.*, 241, 177–193, 2001.
- Hu, R.: Hydraulic tomography: a new approach coupling hydraulic travel time, attenuation and steady shape inversions for high-spatial resolution aquifer characterization, Ph.D. thesis, University of Göttingen, Göttingen, 116 pp., 2011.
- Hubinger, B. and Birk, S.: Influence of initial heterogeneities and recharge limitations on the evolution of aperture distributions in carbonate aquifers, *Hydrol. Earth Syst. Sci.*, 15, 3715–3729, doi:10.5194/hess-15-3715-2011, 2011.
- Hückinghaus, D.: Simulation der Aquifergenese und des Wärmetransports in Karstaquiferen, Tübinger Geowissenschaftliche Arbeiten, C42, Tübingen, 1998.
- Hunter, N. M., Bates, P. D., Horritt, M. S., De Roo, A. P. J., and Werner, M. G. F.: Utility of different data types for calibrating flood inundation models within a GLUE framework, *Hydrol. Earth Syst. Sci.*, 9, 412–430, doi:10.5194/hess-9-412-2005, 2005.
- Jeannin, P.-Y.: Modeling flow in phreatic and epiphreatic karst conduits in the Hölloch cave (Muotatal, Switzerland), *Water Resour. Res.*, 37, 191–200, 2001.
- Khu, S.-T., Madsen, H., and di Pierro, F.: Incorporating multiple observations for distributed hydrologic model calibration: an approach using a multi-objective evolutionary algorithm and clustering, *Adv. Water Resour.*, 31, 1387–1398, 2008.
- Kordilla, J., Sauter, M., Reimann, T., and Geyer, T.: Simulation of saturated and unsaturated flow in karst systems at catchment scale using a double continuum approach, *Hydrol. Earth Syst. Sci.*, 16, 3909–3923, doi:10.5194/hess-16-3909-2012, 2012.
- Kovács, A., Perrochet, P., Király, L., and Jeannin, P.-Y.: A quantitative method for the characterisation of karst aquifers based on spring hydrograph analysis, *J. Hydrol.*, 303, 152–164, 2005.
- Liedl, R., Sauter, M., Hückinghaus, D., Clemens, T., and Teutsch, G.: Simulation of the development of karst aquifers using a coupled continuum pipe flow model, *Water Resour. Res.*, 39, 1057, doi:10.1029/2001WR001206, 2003.

9311

- Li, H. T., Brunner, P., Kinzelbach, W., Li, W. P., and Dong, X. G.: Calibration of a groundwater model using pattern information from remote sensing data, *J. Hydrol.*, 377, 120–130, doi:10.1016/j.jhydrol.2009.08.012, 2009.
- Madsen, H.: Parameter estimation in distributed hydrological catchment modelling using automatic calibration with multiple objectives, *Adv. Water Resour.*, 26, 205–216, 2003.
- Merkel, P.: Karsthydrologische Untersuchungen im Lauchertgebiet (westl. Schwäbische Alb), Diplom thesis, University of Tübingen, Tübingen, 108 pp., 1991.
- Mohrlok, U.: Numerische Modellierung der Grundwasserströmung im Einzugsgebiet der Gallusquelle unter Festlegung eines Drainagesystems, *Grundwasser*, 19, 73–85, doi:10.1007/s00767-013-0249-x, 2014.
- Mohrlok, U. and Sauter, M.: Modelling groundwater flow in a karst terrain using discrete and double-continuum approaches: importance of spatial and temporal distribution of recharge, in: *Proceedings of the 12th International Congress of Speology, 2/6th Conference on Limestone Hydrology and Fissured Media, La Chaux-de-Fonds, Switzerland, 10–17 August 1997*, 167–170, 1997.
- Oehlmann, S., Geyer, T., Licha, T., and Birk, S.: Influence of aquifer heterogeneity on karst hydraulics and catchment delineation employing distributive modeling approaches, *Hydrol. Earth Syst. Sci.*, 17, 4729–4742, doi:10.5194/hess-17-4729-2013, 2013.
- Ophori, D. U.: Constraining permeabilities in a large-scale groundwater system through model calibration, *J. Hydrol.*, 224, 1–20, 1999.
- Rehrl, C. and Birk, S.: Hydrogeological characterisation and modelling of spring catchments in a changing environment, *Aust. J. Earth Sci.*, 103, 106–117, 2010.
- Reiber, H., Klein, F., Selg, M., and Heidland, S.: Hydrogeologische Erkundung Baden-Württemberg – Mittlere Alb 4 – Markierungsversuche, Abwassereinleitungen, Landesamt für Umwelt, Messungen und Naturschutz Baden-Württemberg, Tübingen, 71 pp., 2010.
- Reimann, T., Rehrl, C., Shoemaker, W. B., Geyer, T., and Birk, S.: The significance of turbulent flow representation in single-continuum models, *Water Resour. Res.*, 47, W09503, doi:10.1029/2010WR010133, 2011.
- Sauter, M.: Quantification and Forecasting of Regional Groundwater Flow and Transport in a Karst Aquifer (Gallusquelle, Malm, SW Germany), Tübinger Geowissenschaftliche Arbeiten, C13, Tübingen, 1992.

9312

- Strayle, G.: Karsthydrologische Untersuchungen auf der Ebinger Alb (Schwäbischer Jura), in: Jahreshefte des Geologischen Landesamtes Baden-Württemberg, 12, Freiburg im Breisgau, 1970.
- 5 Teutsch, G. and Sauter, M.: Groundwater Modeling in karst terranes: scale effects, data acquisition and field validation, in: Proceedings of the 3rd Conference on Hydrogeology, Ecology, Monitoring and Management of Ground Water in Karst Terranes, 4–6 December 1991, Nashville, USA, 17–34, 1991.
- 10 Villinger, E.: Über Potentialverteilung und Strömungssysteme im Karstwasser der Schwäbischen Alb (Oberer Jura, SW-Deutschland), Geologisches Jahrbuch, C18, Bundesanstalt für Geowissenschaften und Rohstoffe und Geologische Landesämter der Bundesrepublik Deutschland, Hannover, 1977.
- Villinger, E.: Hydrogeologie, in: Erläuterungen zu Blatt 7721 Gammertingen, Geologische Karte 1 : 25 000 von Baden-Württemberg, edited by: Gwinner, M. P., Geologisches Landesamt Baden-Württemberg, Freiburg/Stuttgart, 30–57, 1993.
- 15 Worthington, S. R. H.: Diagnostic hydrogeologic characteristics of a karst aquifer (Kentucky, USA), *Hydrogeol. J.*, 17, 1665–1678, doi:10.1007/s10040-009-0489-0, 2009.

9313

**Table 1.** Field data of the simulated tracer tests.

|   | Tracer test 1 | Tracer test 2 |
|---|---------------|---------------|
| input mass (kg)                                 | 0.75          | 10            |
| recovery (%)                                    | 72            | 50            |
| distance to spring (km)                         | 3             | 10            |
| spring discharge ( $\text{m}^3 \text{s}^{-1}$ ) | 0.375         | 0.76          |
| sampling interval                               | 1 min         | 6 h           |
| peak time (h)                                   | 47            | 79.5          |

9314

**Table 2.** Specifics of the different scenarios. The bold writing indicates the parameter that is analysed in the respective scenario. Details to the scenarios can be found in Sect. 4.

| Parameter                    | Scenario 1 | Scenario 2             | Scenario 3      | Scenario 4      | Scenario 5                   |
|------------------------------|------------|------------------------|-----------------|-----------------|------------------------------|
| $K_c$                        | constant   | <b>linear increase</b> | linear increase | linear increase | linear increase              |
| lateral network              | minimal    | minimal                | <b>extended</b> | minimal         | minimal                      |
| $K_m$                        | constant   | constant               | constant        | <b>variable</b> | constant                     |
| intersection radius $r_{c2}$ | $r_{c0}$   | $r_{c0}$               | $r_{c0}$        | $r_{c0}$        | $\sqrt{r_{c0}^2 + r_{c1}^2}$ |

9315

**Table 3.** Parameters for the two different conduit configurations compared in scenario 4.  $b$  is the minimum conduit radius,  $m$  the slope of radius increase towards the springs,  $b_h$  the highest conduit roughness,  $m_h$  the slope of roughness decrease away from the spring and  $V$  the conduit volume.

|                            | Geometry 1            | Geometry 2           |
|----------------------------|-----------------------|----------------------|
| $b$ (m)                    | 0.01                  | 0.5                  |
| $m$ (-)                    | $2.07 \times 10^{-4}$ | $1.5 \times 10^{-4}$ |
| $b_h$ ( $s^{-1} m^{1/3}$ ) | 0.17                  | 0.15                 |
| $m_h$ (-)                  | 0.4                   | 0.6                  |
| $V$ ( $m^3$ )              | 112 564               | 153 435              |

9316

**Table 4.** Calibrated and simulated parameters for the best-fit simulations. Literature values are given if available. TT1 and TT2 refer to the two tracer tests.

| Parameter                                | Simulated values scenario 2 | Simulated values scenario 5 | Literature values   |
|--|-----------------------------|-----------------------------|---|
| $K_m$ ( $\text{m s}^{-1}$ )              | $8 \times 10^{-6}$          | $1.5 \times 10^{-5}$        | $1 \times 10^{-6}$ – $2 \times 10^{-5}$<br>(local scale) <sup>e</sup><br>$2 \times 10^{-5}$ – $1 \times 10^{-4}$<br>(regional scale) <sup>e</sup> |
| $m_h$ (–)                                | 0.3                         | 0.3                         | –   |
| $b_h$ ( $\text{m}^{1/3} \text{s}^{-1}$ ) | 0.22                        | 0.18                        | –   |
| $n$ ( $\text{s m}^{-1/3}$ )              | 1.04–4.55                   | 1.05–5.56                   | 0.03–1.07 <sup>a</sup>  |
| $b$ (m)                                  | 0.01                        | 0.01                        | –   |
| $m$ (–)                                  | $2.04 \times 10^{-4}$       | $1.42 \times 10^{-4}$       | –   |
| $\varepsilon_1$ (m) for TT 1             | 7.15                        | 7.5                         | $4.4$ – $6.9$ <sup>f</sup> , $10$ <sup>e</sup>  |
| $\varepsilon_2$ (m) for TT 2             | 30                          | 23                          | $20$ <sup>g</sup>   |
| $A$ ( $\text{m}^2$ )                     | 19.1                        | 21                          | $13.9$ <sup>f</sup>   |
| $V$ ( $\text{m}^3$ )                     | 109 351                     | 89 2867                     | $\leq 200\,000$ <sup>b</sup>  |
| RMSE H (m)                               | 5.61                        | 5.91                        | –   |
| Peak offset TT 1 (h)                     | $-0.28$ <sup>c</sup>        | $-0.28$ <sup>c</sup>        | –   |
| Peak offset TT 2 (h)                     | $2.5$ <sup>d</sup>          | $-1.39$ <sup>d</sup>        | –   |

<sup>a</sup> Jeannin (2001);  
<sup>b</sup> Geyer et al. (2008);  
<sup>c</sup> measurement interval 1 min, simulation interval 2.7 h;  
<sup>d</sup> measurement interval 6 h, simulation interval 2.7 h;  
<sup>e</sup> Sauter (1992);  
<sup>f</sup> Birk et al. (2005);  
<sup>g</sup> Merkel (1991).

9317

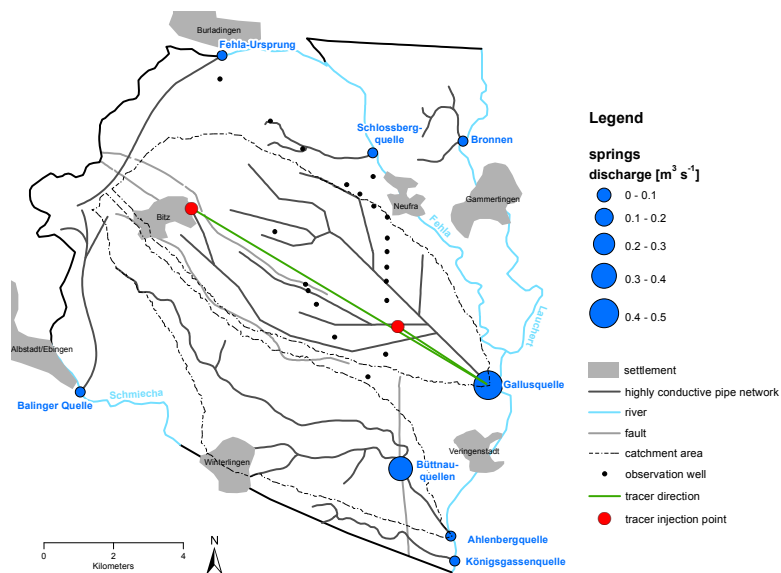


**Figure 1.** Plan view of the model area. Settlements, fault zones and rivers in the area are plotted, as well as the 20 observation wells used for hydraulic head calibration, the six springs used for spring discharge calibration and the two tracer tests employed for flow velocity calibration. Catchment areas for the Gallusquelle spring and the Ahlenberg- and Büttnauquellen springs were simulated after Oehlmann et al. (2013).

9318

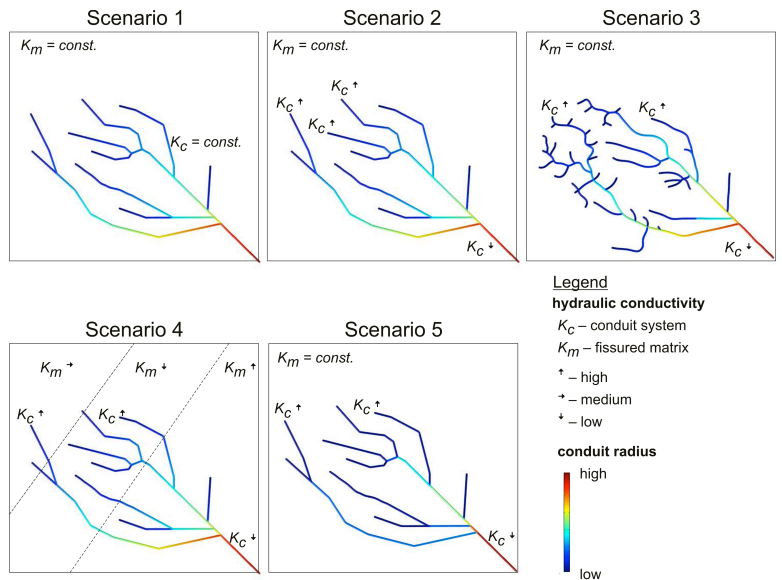


**Figure 2.** Conceptual overview of the simulated scenarios. The conduit geometry and the varied parameters are shown.

9319

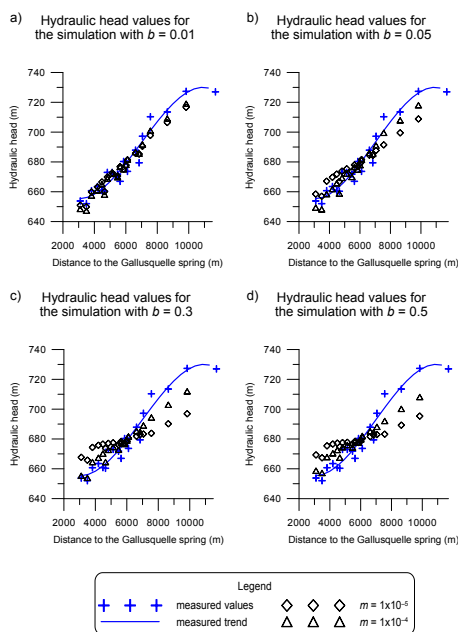


**Figure 3.** Hydraulic head distributions for different combinations of geometric conduit parameters.  $b$  is the lowest conduit radius and  $m$  the radius increase along the conduit. For comparison, a trend-line is fitted to the measured hydraulic head values showing the distribution of hydraulic gradients from the Gallusquelle spring to the western border of its catchment area.

9320

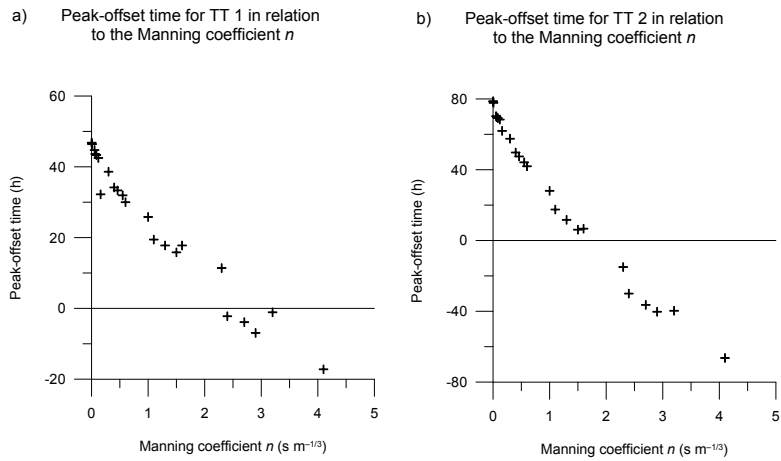


**Figure 4.** Difference between peak concentration times vs. the Manning  $n$  value. High  $n$  values correspond to high conduit volumes and high cross-sectional areas at the spring (a) for tracer test 1 (b) for tracer test 2.

9321

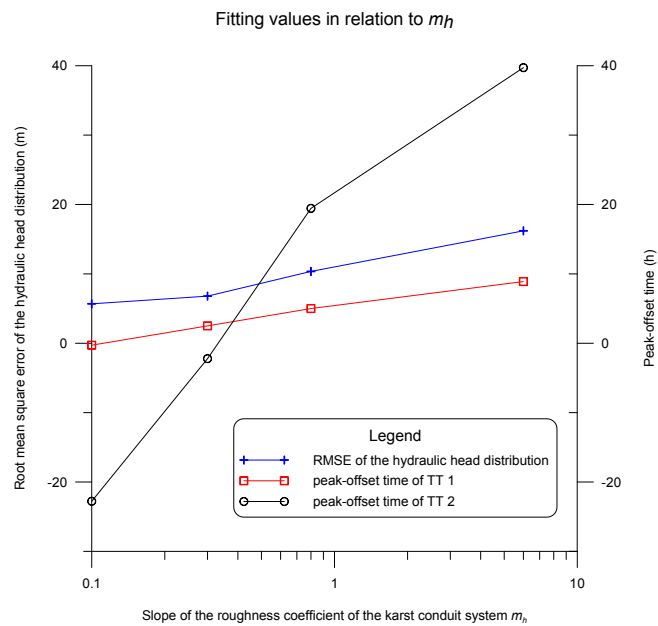


**Figure 5.** Hydraulic head errors and differences between peak concentration times for both tracer tests shown for a conduit geometry with a starting value  $b = 0.01$  m and a radius increase of  $m = 2 \times 10^{-4}$ . Each  $m_h$  value corresponds to a respective value of the highest conduit roughness  $b_h$  and each combination results in the same spring discharge.

9322

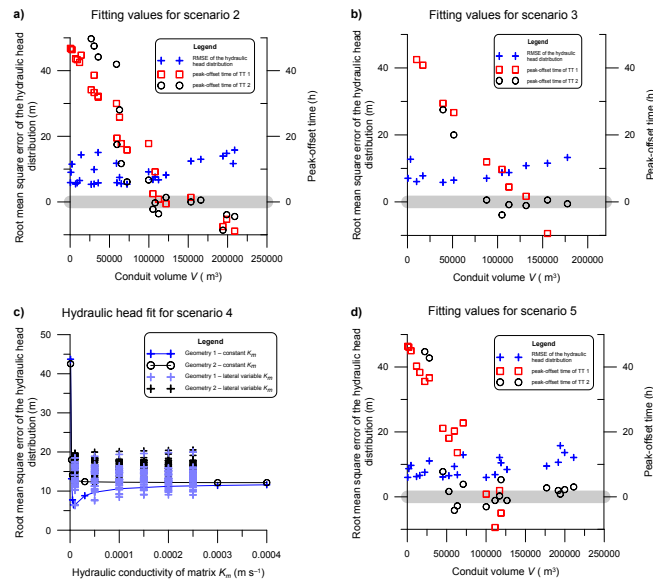


**Figure 6.** Calibrated values for the simulated scenarios. For scenarios 2, 3 and 5 (**a**, **b** and **d**) hydraulic head fit and the peak-offset times of both tracer tests (referred to as TT1 and TT2) are shown in relation to conduit volume. The thick grey bar marks the target value of zero. For scenario 4 (**c**) the root mean square error of the hydraulic heads is given for two different conduit geometries in relation to the hydraulic conductivity of the fissured matrix  $K_m$ . For the version with laterally variable matrix conductivity the axis shows as an example the hydraulic conductivity of the north-western part. The parameters for the two geometries are given in Table 3.

9323

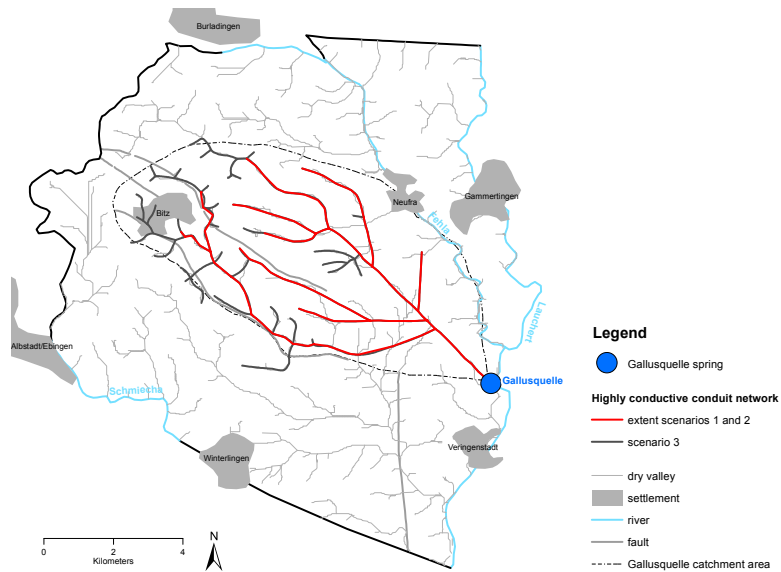


**Figure 7.** Extended conduit system for scenario 3. The conduit configuration (extent) that is used for the other scenarios is marked in red.

9324



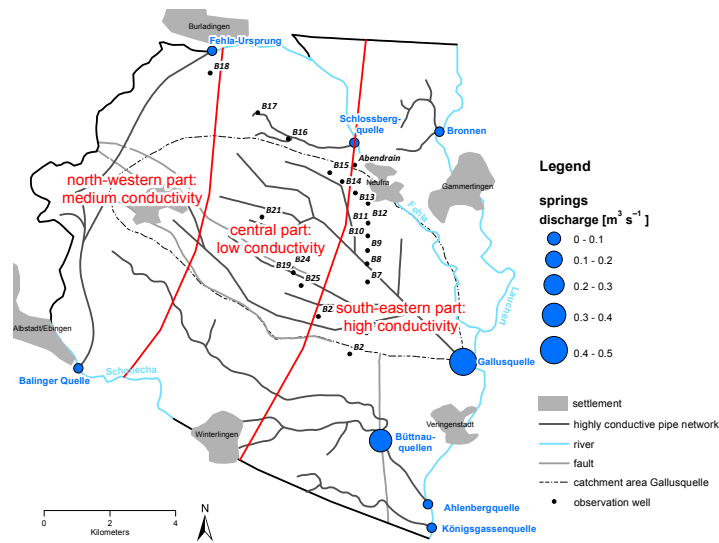


**Figure 8.** Model catchment with spatially distributed hydraulic conductivities. The model area is divided into three parts after geologic aspects. For each segment different values of the hydraulic conductivity were examined during parameter analysis.

9325

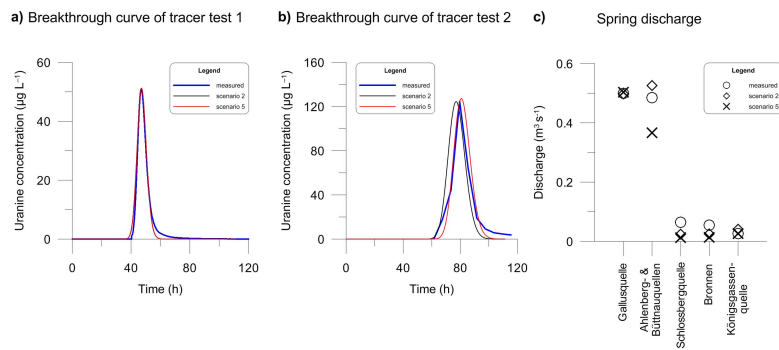


**Figure 9.** Comparison of the best-fit simulations with field data. **(a)** Breakthrough curve of tracer test 1, **(b)** breakthrough curve of tracer test 2, **(c)** spring discharge.

9326